# RADIAL BASIS FUNCTION AIDED TURBO EQUALISATION OF TCM, TTCM, BICM AND BICM-ID ASSISTED WIRELESS TRANSCEIVERS

*S. X. Ng, M. S. Yee and L. Hanzo*

**Invited Paper**
School of ECS, Univ. of Southampton, SO17 1BJ, UK.
Tel: +44-23-8058 3125, Fax:+44-23-8058 4508
Email:lh@ecs.soton.ac.uk, http://www-mobile.ecs.soton.ac.uk

**Abstract:** *Following a brief portrayal of the state-of-the-art a range of Coded Modulation (CM) assisted Radial Basis Function (RBF) based Turbo Equalisation (TEQ) schemes are investigated when communicating over dispersive Rayleigh fading channels. Furthermore, a reduced complexity RBF TEQ is proposed, which is referred to as an Inphase/Quadrature-phase RBF Turbo Equaliser (I/Q-RBF-TEQ). It is demonstrated that the I/Q-RBF-TEQ is capable of reducing the associated implementational complexity by equalising the I and Q components of a complex-valued phasor constellation separately. It is demonstrated that the detrimental effects of this seemingly flawed simplification may be eliminated with the aid of the proposed low-complexity turbo equaliser. The I/Q-RBF-TEQ employs iterative channel estimation and it is capable of attaining the same performance, as the significantly more complex conventional turbo equaliser. The attainable coding gain of the various CM schemes increased substantially, when employing the proposed RBF-TEQ or RBF-I/Q-TEQ, rather than the conventional non-iterative Decision Feedback Equaliser (DFE). The best overall performer was the RBF-I/Q-TEQ-TTCM scheme, requiring only 1.88 dB higher SNR at a BER of $10^{-5}$, than the identical throughput 3 BPS uncoded 8PSK scheme communicating over an AWGN channel. The coding gain of the scheme was 16.78 dB.*

**Keywords:** RBF, I/Q, TEQ, CM, TCM, TTCM, BICM, BICM-ID.

## 1. INTRODUCTION

Maintaining a high spectral efficiency is of salient importance in mobile communication systems owing to the paucity and high price of the radio spectrum. For the sake of efficiently exploiting the available radio spectrum, joint coding and modulation or Coded Modulation (CM) schemes were first proposed by Ungerböck in 1982 [1] for non-dispersive Gaussian channels. The benefit of TCM is that it is capable of achieving a coding gain in comparison to uncoded transmissions by expanding the modulation phasor constellation and hence absorbing the parity bits without bandwidth expansion, when transmitting over non-dispersive Gaussian channels. Ungerböck's contribution motivated intensive research on the topic, especially after the conception of turbo codes by Berrou *et al.* [2], leading to Turbo TCM (TTCM) invented by Robertson and Wörz [3]. Further advances were made in the context of designing CM schemes for wireless Rayleigh fading channels by Zehavi [4], by Caire, Taricco and Biglieri [5] in the context of Bit-Interleaved Coded Modulation (BICM) as well as by Li and Ritcey [5], leading to the concept of iteratively decoded BICM (BICM-ID). All of these CM methods are studied in [6]. In this contribution non-linearly detected reduced-complexity turbo-equalised TCM, TTCM, BICM and BICM-ID will be studied, when communicating over frequency selective wireless channels.

The Radial Basis Function (RBF) based channel equalisers proposed by Chen *et al.* [7] constitute an efficient family of non-linear channel equalisation schemes, especially in the context of hostile non-minimum-phase wireless channels, where the received phasor constellations may become linearly non-separable and hence conventional equalisers [8] exhibit an resudual error floor. RBF equalisers formulate the channel equalisation procedure as a classification problem. More explicitly, in conventional equalisers [8, 9] the received signal is linearly filtered with the aid of the channel equaliser, which intends to mimic the inverse of the Channel's Impulse Response (CIR). By contrast, given the CIR, the RBF based equaliser determines all possible channel outputs engendered by the set of legitimate transmitted symbols and then classifies each received symbol into the nearest legitimate channel output, which allows us to infer the specific symbol transmitted. Following a brief lull in the field after the seminal contributions of Chen *et al.* [7], recently the application of non-linear RBF based equalisers has been studied in conjunction with turbo channel codecs [10,11], adaptive modulation [11,12], space-time codecs [11,13] as well as turbo equalisation [6,11,14]. Various turbo equalisers were comparatively studied in [6, 15].

In this contribution a CM-aided reduced complexity RBF

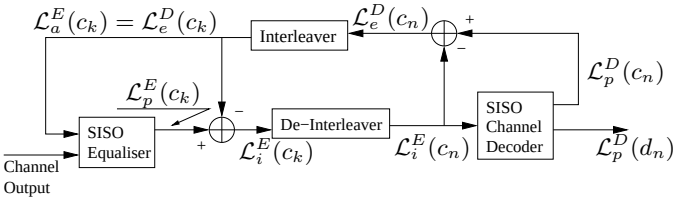


Figure 1: Iterative turbo equalisation schematic

TEQ is advocated, which we refer to as an In-phase/Quadrature-phase RBF Turbo Equaliser (I/Q-RBF-TEQ), since it equalises the I and Q components of a complex-valued phasor constellation separately, despite their interdependence imposed by their convolution with the complex-valued CIR [16]. It is shown that the detrimental effects of this seemingly flawed simplification may be eliminated with the aid of the proposed low-complexity TEQ. The I/Q-RBF-TEQ is also assisted by iterative channel estimation.

The remainder of this paper is organised as follows. The philosophy of the RBF-TEQ based CM scheme is presented in Section 2, while the reduced-complexity RBF-I/Q-TEQ based CM scheme is proposed in Section 3. Finally, we will conclude in Section 4.

## 2. RBF-AIDED TURBO EQUALISATION

Turbo equalisation was proposed by Douillard *et. al.* [17] for a convolutional coded Binary Phase Shift Keying (BPSK) system [6]. Its basic schematic is illustrated in Figure 1, where we have used the notation $\mathcal{L}^E$ and $\mathcal{L}^D$ for denoting the Log-domain Probability (LP) values output by the SISO equaliser and SISO decoder, respectively. The subscripts $e$, $i$, $a$ and $p$ were used to represent the extrinsic LP, the combined channel and extrinsic LP, the *a priori* LP and the *a posteriori* LP, respectively. Referring to Figure 1, the SISO equaliser processes the channel outputs and the *a priori* information $\mathcal{L}_a^E(c_k)$ of the coded symbol, and generates the *a posteriori* LP values $\mathcal{L}_p^E(c_k)$ of the interleaved coded symbol $c_k$ seen in Figure 2. Before passing the above *a posteriori* LPs generated by the SISO equaliser to the SISO decoder of Figure 1, the contribution of the decoder — which is represented in the form of the *a priori* information $\mathcal{L}_a^E(c_k)$ — accruing from the previous iteration must be removed, in order to yield the combined channel and extrinsic information $\mathcal{L}_i^E(c_k)$ seen in Figure 1. Gertsman and Lodge [18] exploited these advances and demonstrated that the iterative process of turbo equalisation is capable of compensating for the performance degradation imposed by imperfect channel estimation. In [19] turbo equalisation was implemented by Raphaeli and Zarai in conjunction with turbo coding, rather than conventional convolutional coding. The principles of bit-based iterative turbo decoding [2] were appropriately modified for employment in the symbol-based M-ary coded modulation system of Figure 2.

The RBF network based equaliser is capable of utilising the *a priori* information $\mathcal{L}_a^E(c_k)$ provided by the channel decoder of Figure 1, in order to improve its performance. This *a priori* information can be assigned namely to the weights of the RBF network [20]. In turn, the RBF equaliser provides the decoder with the *a posteriori* information $\mathcal{L}_p^E(c_k)$ concerning the coded symbol. We will now provide a brief overview of symbol-based coded modulation assisted, RBF aided turbo equalisation. Note that this procedure is different from the separate bit-based channel coding and modulation philosophy outlined in Section 11.2 of [11].

### 2.1. System Overview

The conditional Probability Density Function (PDF) of the $i$th symbol, $i = 1, \ldots, \mathsf{M}$, associated with the $i$th subnet of the M-ary RBF channel equaliser having a feedforward order of $m$ is given by [11]:

$$f_{RBF}^i(\mathbf{v}_k) = \sum_{j=1}^{n_{s,i}} P(\mathbf{r}_j^i)(2\pi\sigma_N^2)^{-m/2} \exp\left(\frac{-|\mathbf{v}_k - \mathbf{r}_j^i|^2}{2\sigma_N^2}\right) \quad i = 1, \ldots, \mathsf{M}, \qquad j = 1, \ldots, n_{s,i} \tag{1}$$

where

$$w_j^i = P(\mathbf{r}_j^i)(2\pi\sigma_N^2)^{-m/2} \tag{2}$$

is the RBF's weight and

$$\varphi(x) = \exp\left(\frac{-x^2}{2\sigma_N^2}\right) \tag{3}$$

is the activation function [11]. Furthermore, $\mathbf{r}_j^i$ are the RBF's centres, which are assigned the values of the channel output states in order to arrive at the Bayesian equalisation solution [11, 21], $\mathbf{v}_k$ is the received symbol sequence and $\sigma_N^2$ is the noise variance of the channel. The actual number of channel states $n_{s,i}$ is determined by the specific design of the algorithm invoked, but in general we aim for reducing the number of channel states from the optimum number of $n_{s,i} = \mathsf{M}^{m+\bar{L}-1}$, where $m$ is the equaliser's feedforward order and $\bar{L}+1$ is the CIR duration [22–24], to a lower value for the sake of reducing the computational complexity.

The term $\mathbf{v}_k$ in (1) is the received symbol sequence, as shown in Figure 2. Explicitly, $\mathbf{v}_k$ consists of the channel outputs observed by the $m$th order equaliser, which can be expressed in an $m$-dimensional vectorial form as:

$$\mathbf{v}_k = \begin{bmatrix} v_k & v_{k-1} & \ldots & v_{k-m+1} \end{bmatrix}^T. \tag{4}$$

The channel input state associated with the $i$th subnet of the M-ary RBF channel equaliser is given by the vector $\mathbf{s}_j^i$, which is also referred to as the channel input vector. Explicitly, this vector consists of the $j$th possible combination of the $(\bar{L}+m)$ number of transmitted symbols, namely by:

$$\mathbf{s}_j^i = \left[s_{j1} \ldots s_{j(\tau+1)} = g(i) \ldots s_{jp} \ldots s_{j(\bar{L}+m)}\right]^T, \tag{5}$$

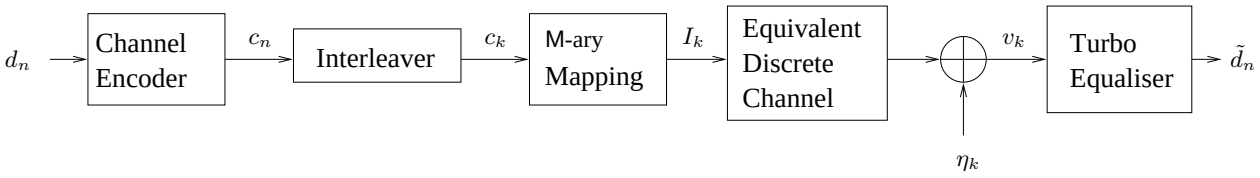


Figure 2: Serially concatenated coded M-ary system using the turbo equaliser, which performs the equalisation, demodulation and channel decoding iteratively.

where $\tau$ is the equaliser's decision delay and $g(i)$ translates the $i$th M-ary symbol to the complex plane. The channel output state $\mathbf{r}_j^i$ associated with the $i$th subnet of the M-ary RBF channel equaliser is the product of the CIR matrix $\mathbf{H}$ and the channel input states $\mathbf{s}_j^i$. The variable $\mathbf{r}_j^i$ is also referred to as the channel output vector and it is expressed as [11]:

$$\mathbf{r}_j^i = \mathbf{H}\mathbf{s}_j^i, \tag{6}$$

where the z-transform of the CIR $h(t)$ having a memory of $\bar{L}$ symbols is represented by $H(z) = \sum_{n=0}^{\bar{L}} h_n z^{-n}$ and $\mathbf{H}$ is an $m \times (m + \bar{L})$ matrix given by the CIR taps as follows:

$$\mathbf{H} = \begin{bmatrix} h_0 & h_1 & \dots & h_{\bar{L}} & \dots & 0 \\ 0 & h_0 & \dots & h_{\bar{L}-1} & \dots & 0 \\ \vdots & \vdots & & & & \vdots \\ 0 & \dots & h_0 & \dots & h_{\bar{L}-1} & h_{\bar{L}} \end{bmatrix}. \tag{7}$$

The RBF weights $w_j^i$ correspond to the *a priori* probability of the channel states $P(\mathbf{r}_j^i)$, $i = 1, \dots, \mathsf{M}$, $j = 1, \dots, n_{s,i}$, as shown in (2). The probability of the channel states $P(\mathbf{r}_j^i)$, and therefore the weights of the RBF equaliser can be derived from the *a priori* information $\mathcal{L}_a^E(c_k)$ estimated by the symbol-based MAP channel decoder. Explicitly, $\mathcal{L}_a^E(c_k)$ is the interleaved version of the extrinsic information given by:

$$\mathcal{L}_e^D(c_n) = \mathcal{L}_p^D(c_n) - \mathcal{L}_i^E(c_n). \tag{8}$$

Based on (6) – assuming a time-invariant CIR and that the symbols in the sequence $\mathbf{s}_j^i$ are statistically independent of each other with the advent of using the interleaver – the probability of the received channel output states $\mathbf{r}_j^i$ is given by:

$$\begin{aligned} P(\mathbf{r}_j^i) &= P(\mathbf{s}_j^i) \\ &= P(s_{j1} \cap \dots s_{j(\tau+1)} \\ &\quad = g(i) \cap \dots s_{jp} \cap \dots s_{j(\bar{L}+m)}) \\ &= \prod_{p=1}^{\bar{L}+m} P(s_{jp}) \qquad (9) \\ &= \prod_{p=1}^{\bar{L}+m} \exp\left(\mathcal{L}_a^E(s_{jp} = c_{k-p+1})\right), \\ &\qquad j = 1, \dots, n_{s,i}, \end{aligned} \tag{10}$$

where the transmitted symbol vector component $s_{jp}$ – i.e. the $p$th symbol in the vector of (5) – is given by $\mathsf{m} = \log_2 \mathsf{M}$ number of bits $b_{jp1}, b_{jp2}, \dots, b_{jp\mathsf{m}}$, which constitute the coded symbol $c_{k-p+1}$. Explicitly, the transmitted symbol vector component $s_{jp}$ is mapped to the coded symbol $c_{k-p+1}$.

In summary, the computation of the PDF $f_{RBF}^i(\mathbf{v}_k)$ of the $i$th symbol in (1), $i = 1, \dots, \mathsf{M}$, which is associated with the $i$th subnet of the M-ary RBF channel equaliser, requires the knowledge of the channel states' *a priori* probability $P(\mathbf{r}_j^i)$, when determining the RBF weights $w_j^i$, as shown in (2). Finally, $P(\mathbf{r}_j^i)$ can be computed from (10) using the *a priori* information $\mathcal{L}_a^E(c_k)$. Explicitly, $\mathcal{L}_a^E(c_k)$ is the interleaved version of the extrinsic information given by Equation 8 and the *a posteriori* information $\mathcal{L}_p^D(c_n)$ is obtained from the channel decoder. Therefore, we have demonstrated how the soft output $\mathcal{L}_a^E(c_k)$ provided by the symbol-based MAP channel decoder of Figure 1 can be utilised by the RBF equaliser.

On the other hand, the $i$th subnet of the M-ary RBF equaliser provides the *a posteriori* LP $\mathcal{L}_p^E$ value of the $i$th coded symbol $c_k^i$ according to:

$$\mathcal{L}_p^E(c_k^i) = \ln\left(\frac{f_{RBF}^i(\mathbf{v}_k)}{\sum_{l=1}^{\mathsf{M}} f_{RBF}^l(\mathbf{v}_k)}\right), \tag{11}$$

where $f_{RBF}^i(\mathbf{v}_k)$ was defined by (1), while $\sum_{l=1}^{\mathsf{M}} f_{RBF}^l(\mathbf{v}_k)$ is a normalisation factor, resulting in $\sum_{i=1}^{\mathsf{M}} \exp(\mathcal{L}_p^E(c_k^i)) = 1$ and the received sequence $\mathbf{v}_k$ is defined in (4).

### 2.2. Performance of the RBF-aided TEQ

We employed the Jacobian RBF-DFE of [10, 11], which reduced the complexity of the RBF equaliser by utilising the Jacobian logarithmic function [25], and decision feedback assisted RBF-centre selection [11, 20] as well as a TEQ scheme using a symbol-based MAP channel decoder. The RBF-DFE based TEQ is specified by the equaliser's decision delay $\tau$, the feedforward order $m$ and the feedback order $n$. Specifically, we employed $\tau$=2, $m$=3 and $n$=1. The transmitted $(\mathsf{m}-1)$-bit information symbols are encoded by a rate-$(\mathsf{m}-1)/\mathsf{m}$ CM encoder, interleaved and mapped to an M-ary modulated symbol where $\mathsf{M} = 2^{\mathsf{m}}$. In this study we utilised 16QAM in order to obtain an effective transmission throughput of $\mathsf{m} - 1$=3 information Bits

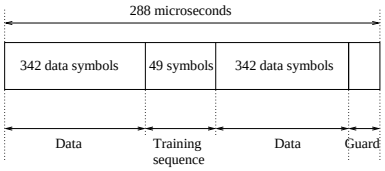


non-spread data burst

Figure 3: Transmission burst structure of the FMA1 non-spread speech burst of the FRAMES proposal [26].

Per Symbol (BPS). All the 16QAM-based CM schemes employed exhibited a similar decoding complexity for the sake of a fair comparison. More specifically, a component TCM (or BICM) code memory of 3 was used for the TTCM (or BICM-ID) scheme. The number of iterations for TTCM (BICM-ID) was fixed to 4 (8). Hence, the iterative scheme exhibited a similar decoding complexity to that of the TCM (BICM) code of memory 6 when quantified in terms of the number of coding states [6].

The transmission burst structure used in this system is the FMA1 non-spread data burst specified by the Pan-European FRAMES proposal [26], which is shown in Figure 3. When considering a Time Division Multiple Access (TDMA) system having 16 slots per $4.615ms$ TDMA frame, the transmission burst length is 288 $\mu s$, as shown in Figure 3. In our investigations, the transmission delay was limited to approximately $8 \times 4.615ms = 37ms$. This corresponds to a transmission delay of 8 TDMA frames, resulting in a maximum channel interleaver depth of $8 \times 684 = 5472$ symbols can be employed.

A two-path, symbol-spaced CIR of equal tap weights was used, which can be expressed as $h(t) = 0.707 + 0.707z^{-1}$, where $\bar{L} = 1$ and the Rayleigh fading statistics obeyed a normalised Doppler frequency of $3.25 \times 10^{-5}$. The fading magnitude and phase was kept constant for the duration of a transmission burst, a condition which we refer to as employing transmission burst-invariant fading. The Least Mean Square (LMS) algorithm [27] was employed for estimating the CIR based on the training sequence of the transmission burst, as seen in Figure 3. Iterative CIR estimation was invoked, where the initial LMS CIR estimation step-size used was 0.05, which was reduced to 0.01 for the second and the subsequent iterations. This LMS-aided CIR estimation was outlined in [11].

Figure 4 illustrates the BER and FER versus Signal to Noise Ratio (SNR) per information bit, namely $E_b/N_0$ performance of the RBF-TEQ scheme assisted by 16QAM-based TCM, TTCM, BICM and BICM-ID, when communicating over a dispersive channel having an equally-weighted two-path Rayleigh fading CIR and utilising iterative LMS-based CIR estimation. The iteration gains of TEQ can be observed by comparing the performance of the first and third TEQ iteration of the systems. The BER and FER performance of the identical-throughput uncoded 8PSK scheme communicating over non-dispersive AWGN channels was

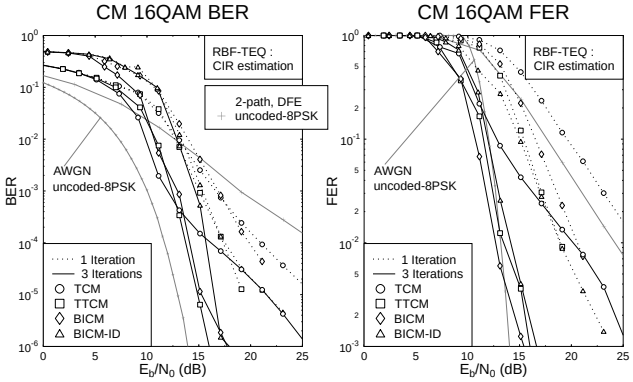


Figure 4: The BER and FER versus $E_b/N_0$ performance of the **RBF-TEQ for various CM** 16QAM schemes, when communicating over the dispersive channel having an equally-weighted two-path Rayleigh fading CIR.

used as a benchmarker for the 16QAM-based RBF-TEQ arrangement using various CM schemes communicating over the above-mentioned dispersive Rayleigh fading channels. We found in Figure 4 that at a BER of $10^{-5}$, the BER curves of the TTCM, BICM and BICM-ID assisted schemes are only about 2 dB away from the benchmarker. However, as seen in Figure 4 the performance of the TCM assisted scheme improves less rapidly than that of the other schemes, partly owing to the existence of unprotected bits in the TCM coded symbols and partly as a consequence of benefiting from no iterations in case of TCM, as opposed to the inner iterations of TTCM. The BER disadvantage of TCM caused by the unprotected bits is overcome by BICM and BICM-ID, since they protect all bits, while TTCM does not, but nonetheless benefits from inner iterations. On the other hand, the FER performance of the TTCM, BICM and BICM-ID assisted RBF-TEQ schemes was found in Figure 4 to be better than that of the benchmarker at low SNR values. Furthermore, it was found from our simulations that the achievable performance gain remained only marginal when more than three TEQ iterations were employed. It is illustrated in Figure 4 that the RBF-TEQ-BICM scheme attained the highest TEQ gain compared to its counterparts. The RBF-TEQ-BICM scheme is also the best performer in terms of the achievable FER, but the RBF-TEQ-TTCM arrangement has the edge in terms of the BER attained.

In order to compare the performance of the RBF-TEQ assisted CM scheme to that of the conventional DFE assisted CM scheme, we have plotted in Figure 5 the BPS throughput versus $E_b/N_0$ performance of the RBF-TEQ assisted CM-16QAM scheme at BER=$10^{-5}$ when employing LMS CIR estimation and that of the conventional DFE assisted CM-16QAM scheme assuming perfect CIR knowledge, when communicating over the two-path Rayleigh fading channel. The conventional DFE's feedforward order $m$ and feedback order $n$ were set to seven and one, respectively, since we found from our simulations that further increasing the values of $m$ and $n$ yielded no signifi-

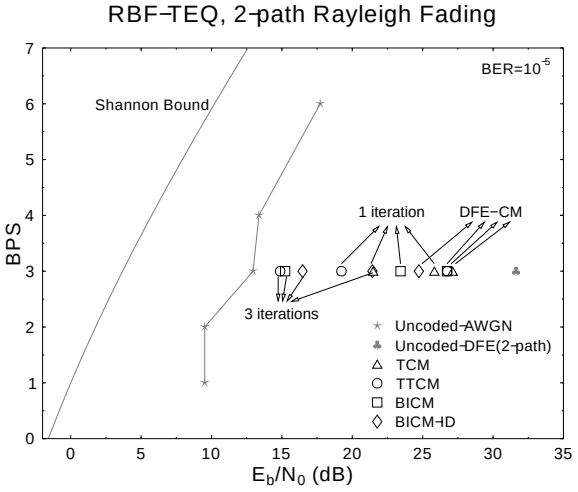


Figure 5: The BPS throughput versus $E_b/N_0$ performance at BER=$10^{-5}$ of the **RBF-TEQ for various CM** 16QAM schemes, when communicating over the dispersive channel having an equally-weighted two-path Rayleigh fading CIR.

cant performance improvement when communicating over the two-path Rayleigh fading channel. Specifically, the conventional DFE exhibits a lower complexity than that of the RBF-DFE. However, the BER performance of the conventional DFE scheme is lower than that of its RBF-DFE counterpart owing to experiencing an error floor in the high SNR region [11]. From Figure 5 we notice that the conventional DFE assisted CM-16QAM schemes exhibited approximately 4 to 7 dB coding gain compared to the identical-throughput conventional DFE assisted uncoded-8PSK scheme at a BER of $10^{-5}$. However, the achievable coding gain of the various CM schemes was significantly increased when the RBF-TEQ scheme was employed, although this was achieved at a higher complexity owing to employing an increased number of iterations. Explicitly, a coding gain ranging from 10 to 17 dB was achievable at a BER of $10^{-5}$ by the various CM schemes against the identical-throughput conventional DFE assisted uncoded-8PSK scheme, when the RBF-TEQ scheme used 3 iterations.

Having studied the performance of the RBF-TEQ arrangement employing various CM schemes, let us now commence our discourse on employing CM schemes in the context of the reduced complexity In-phase/Quadrature-phase TEQ system to be described in Section 3.1.

## 3. RBF ASSISTED REDUCED COMPLEXITY I/Q TURBO EQUALISATION

### 3.1. Principle of I/Q Equalisation

We denote the modulated signal by $s(t)$, which is transmitted over the dispersive channel characterised by the Channel Impulse Response (CIR) $h(t)$. The signal is also contaminated by Additive White Gaussian Noise (AWGN) $n(t)$ exhibiting a variance of $\sigma^2 = N_0/2$, where $N_0$ is the single-sided noise power spectral density. The received signal $r(t)$ is then formulated as [6, 28]:

$$\begin{aligned} r(t) &= s(t) * h(t) + n(t) \\ &= [s_I(t) + js_Q(t)] * [h_I(t) + jh_Q(t)] \\ &+ n_I(t) + jn_Q(t) \\ &= r_I(t) + jr_Q(t), \end{aligned} \tag{12}$$

where we have:

$$\begin{aligned} r_I(t) &= s_I(t) * h_I(t) - s_Q(t) * h_Q(t) + n_I(t) \\ r_Q(t) &= s_I(t) * h_Q(t) + s_Q(t) * h_I(t) + n_Q(t), \end{aligned} \tag{13}$$

since the CIR $h(t)$ is complex-valued and therefore consists of the I component $h_I(t)$ and Q component $h_Q(t)$. On the same note, $s_I(t)$ and $s_Q(t)$ are the I and Q components of $s(t)$, while $n_I(t)$ and $n_Q(t)$ denote the corresponding AWGN components. Both of the received I/Q signals, namely $r_I(t)$ and $r_Q(t)$ of (14) become dependent on both $s_I(t)$ and $s_Q(t)$ owing to the cross-coupling effect imposed by the channel having a complex CIR. Hence, a conventional channel equaliser, regardless of whether it is an iterative or non-iterative equaliser, would have to consider the effects of this cross-coupling.

However, it was exploited by Höher in a non-iterative TCM context and it was demonstrated in an iterative turbo-equalised context in [11] that we can compute the $I$ and $Q$ components of the decoupled channel output $r'(t)$, as though they were dependent on $s_I(t)$ or $s_Q(t)$ only, in the context of the following equations [6, 16]:

$$\begin{aligned} {r'}_I(t) &= r_I(t) + \hat{s}_Q(t) * \hat{h}_Q(t) \\ &\quad + j[r_Q(t) - \hat{s}_Q(t) * \hat{h}_I(t)] \\ &= s_I(t) * h_I(t) + n_I(t) \\ &\quad + j[s_I(t) * h_Q(t) + n_Q(t)] \\ &= s_I(t) * h(t) + {n'}_I(t), \\ {r'}_Q(t) &= -r_Q(t) + \hat{s}_I(t) * \hat{h}_Q(t) \\ &\quad + j[r_I(t) - \hat{s}_I(t) * \hat{h}_I(t)] \\ &= -s_Q(t) * h_I(t) - n_Q(t) \\ &\quad + j[-s_Q(t) * h_Q(t) + n_I(t)] \\ &= -s_Q(t) * h(t) + {n'}_Q(t), \end{aligned} \tag{14}$$

where ${n'}_I(t) = n_I(t) + jn_Q(t)$ and ${n'}_Q(t) = -n_Q(t) + jn_I(t)$ are the corresponding noise component for ${r'}_I(t)$ and ${r'}_Q(t)$, respectively. Note that in (14) we have assumed perfect signal regeneration, i.e. $\hat{s}_I(t) = s_I(t)$ and $\hat{s}_Q(t) = s_Q(t)$, as well as perfect channel estimation, i.e. $\hat{h}_I(t) = h_I(t)$ and $\hat{h}_Q(t) = h_Q(t)$, in order to highlight the underlying principle of the reduced complexity equaliser. More explicitly, the removal of the cross-coupling imposed by the complex CIR is facilitated by generating the estimates $\hat{s}_I(t)$ and $\hat{s}_Q(t)$ of the transmitted signal [29] with the aid of the reliability information generated by the channel decoder and then by cancelling the cross-coupling effects imposed by the channel, yielding ${r'}_I(t)$ and ${r'}_Q(t)$,

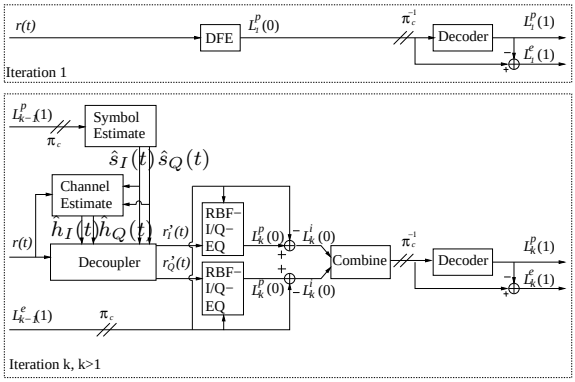


Figure 6: Schematic of the turbo equaliser employing a DFE and a SISO channel decoder in the first turbo equalisation iteration. In subsequent iterations, two RBF-I/Q-EQs and one SISO channel decoder are employed. The notation $\pi_c$ represents a channel interleaver, while $\pi_c^{-1}$ is used to denote a channel deinterleaver.

respectively. In the ideal scenario, where perfect knowledge of both the CIR and that of the transmitted signal is available, it is plausible that the channel-induced cross-coupling between the quadrature components can be removed. However, when unreliable symbol estimates are generated owing to the channel-impaired low-confidence reliability values, errors are introduced in the decoupling operation. Nonetheless, we will show that the associated imperfect decoupling effects are compensated with the aid of the iterative turbo equalisation process in its consecutive iterations.

Following the above decoupling operation, the modified complex channel outputs, namely $r'_I(t)$ and $r'_Q(t)$ of (14), respectively, can be viewed as the result of convolving both quadrature components independently with the complex CIR on each quadrature arm. Consequently, we can equalise $s_I(t)$ and $s_Q(t)$ independently, hence reducing the number of channel states and the associated complexity quite significantly.

In the RBF-I/Q-EQ scheme we utilised the principle of separate I/Q equalisation outlined as in Section 3.1, where two separate RBF equalisers were used for the I and Q component of the transmitted symbols. The in-phase-RBF-EQ has RBF centres, which consist of the in-phase decoupled channel output $r'_I(t)$ of (14) and vice-versa for the quadrature-RBF-EQ. The number of possible channel output states is reduced, since the decoupled channel output $r'(t)$ is dependent on $\sqrt{\mathsf{M}}$ [1] number of possible in-phase or quadrature-phase transmitted symbols instead of the original $\mathsf{M}$ number of possible symbols.

### 3.2. System Overview

Figure 6 illustrates the schematic of the turbo equaliser utilising two reduced-complexity RBF-I/Q equalisers. The same notation are employed here as in Section 2. The subscripts in Figure 6 are used for representing the iteration index, while the argument within the brackets ( ) indicates the index of the receiver stage, where the equalisers are denoted as receiver stage 0, while the channel decoder as receiver stage 1.

The conventional minimum mean square error DFE seen at the top left corner of Figure 6 is used for the first turbo equalisation iteration for providing soft decisions in the form of the LP $L_1^p(0)$ to the CM decoder. Invoking the DFE at the first iteration constitutes a low-complexity approach to providing an initial estimate of the transmitted symbols, as compared to the more complex RBF-I/Q-EQ. The symbol-based MAP channel decoder of Figure 6 generates the *a posteriori* LP $L_1^p(1)$ and from that, the extrinsic information of the encoded symbols $L_1^e(1)$ is extracted. In the next iteration, the *a posteriori* LP $L_1^p(1)$ is used for regenerating estimates of the I and Q components of the transmitted signal, namely $\hat{s}_I(t)$ and $\hat{s}_Q(t)$, as seen in the 'Symbol Estimate' block of Figure 6. The *a posteriori* information was transformed from the logarithmic domain to modulated symbols using the approach employed in [29]. Furthermore, based on the received signal $r(t)$ and the estimated signals $\hat{s}_I(t)$ and $\hat{s}_Q(t)$, the CIR is estimated in the 'Channel Estimate' block to yield $\hat{h}_I(t)$ and $\hat{h}_Q(t)$. The estimated transmitted quadrature components $\hat{s}_I(t)$ and $\hat{s}_Q(t)$ as well as the CIR estimates $\hat{h}_I(t)$ and $\hat{h}_Q(t)$ are then passed to the 'Decoupler' block of Figure 6. At the 'Decoupler' block, $\hat{s}_I(t)$ and $\hat{s}_Q(t)$ are convolved with $\hat{h}_I(t)$ and $\hat{h}_Q(t)$ to yield $\hat{s}_I(t) * \hat{h}_I(t)$, $\hat{s}_I(t) * \hat{h}_Q(t)$, $\hat{s}_Q(t) * \hat{h}_I(t)$ and $\hat{s}_Q(t) * \hat{h}_Q(t)$. These resultant outputs are used for removing the cross-coupling effect seen in (14), from both quadrature components of the received signal $r(t)$, yielding $r'_I(t)$ and $r'_Q(t)$ according to (14).

After the decoupling operation, $r'_I(t)$ and $r'_Q(t)$ are passed to the RBF-I/Q-EQ in the schematic of Figure 6. In addition to these received quadrature signals, the RBF-I/Q-EQ also processes the *a priori* information received, which consists of the extrinsic LPs $L_1^e(1)$ derived from the previous iteration, and generates the *a posteriori* information $L_2^p(0)$. Subsequently, the combined channel and extrinsic information $L_2^i(0)$ is extracted from both RBF-I/Q-EQs in Figure 6 and combined, before being passed to the Log-MAP channel decoder. As in the first turbo equalisation iteration, the *a posteriori* and extrinsic information of the encoded symbol, namely $L_2^p(1)$ and $L_2^e(1)$, respectively, are evaluated. Subsequent turbo equalisation iterations obey the same sequence of operations, until the iteration termination criterion is met.

### 3.3. Performance of the RBF-I/Q-TEQ

In this section, we will study the performance of a number of RBF-I/Q-TEQ schemes employing various CM schemes. Similar simulation parameters to those outlined in Section 2.2 are used. Again, the RBF-DFE based TEQ is specified by the equaliser's decision delay $\tau$, the feedforward order $m$

[1] or approximately $\sqrt{\mathsf{M}}$ for non-square constellations.

and the feedback order $n$. The number of RBF nodes is $n_{s,i} = \bar{\mathsf{M}}^{\bar{L}+m-n}$ and the number of scalar channel states of the Jacobian RBF equaliser is $n_{s,f} = \bar{\mathsf{M}}^{\bar{L}+1}$, where we have $\bar{\mathsf{M}}$=M for the non-I/Q based full-complexity RBF-TEQ system, while $\bar{\mathsf{M}}$=$\sqrt{\mathsf{M}}$ for the I/Q based RBF-TEQ system. Again, M is the constellation size and $\bar{L}+1$ is the CIR duration. The estimated computational complexity of generating the *a posteriori* LP for the Jacobian RBF equaliser is given by [10]: $n_{s,i}(m+2) - 2\bar{\mathsf{M}} + n_{s,f}$ number of additions/subtractions and $2n_{s,f}$ number of multiplications/divisions. Here, we employed $\tau$=2, $m$=3 and $n$=1 for the RBF-TEQ, as well as $m$=7 and $n$=1 for the conventional DFE. Therefore, the 'per-iteration' complexity of the full-RBF-TEQ expressed in terms of the number of additions/subtractions and multiplications/divisions is about 20704 and 512, respectively, while that of the RBF-I/Q-TEQ is about 328 and 32, respectively. Note that in the context of employing 16QAM and communicating over a two-path Rayleigh fading channel, i.e. when $\bar{L} = 1$, the number of RBF nodes in the RBF-TEQ and RBF-I/Q-TEQ are $\mathsf{M}^{\bar{L}+m-n} = 16^3$ and $\sqrt{\mathsf{M}}^{\bar{L}+m-n} = 16^{3/2}$, respectively. For the same system, the trellis-based TEQ schemes such as the SOVA or the max-log MAP equaliser would require a computational complexity on the order of $O(16^2)$, which is comparable to that of the RBF-I/Q-TEQ and is $16^3/16^2 = 16$ times lower than that of the RBF-TEQ. Owing to lack of space, the performance of CM-assisted trellis-based TEQ schemes is not studied in this paper.

Figure 7 illustrates the BER versus $E_b/N_0$ performance of the TTCM assisted RBF-I/Q-TEQ and RBF-TEQ schemes on an iteration by iteration basis. In terms of the attainable BER, the performance of the first three iterations of RBF-I/Q-TEQ-TTCM is inferior to that of the first iteration of RBF-TEQ-TTCM for BER values below $10^{-4}$. This is due to the employment of a conventional DFE during the first iteration of the RBF-I/Q-TEQ-TTCM scheme, as well as owing to the imperfect I/Q decoupling effects, when unreliable symbol estimates are employed. However, as more reliable symbol estimates become available with the aid of the iterative TEQ scheme during the forthcoming iterations, the performance of RBF-I/Q-TEQ-TTCM becomes comparable to that of the full-complexity RBF-TEQ-TTCM arrangement. Eventually, the performance of RBF-I/Q-TEQ-TTCM having eight iterations is identical to that of RBF-TEQ-TTCM having four iterations for BER values below $10^{-4}$, as shown in Figure 7. Note that the complexity imposed by the conventional DFE during the first RBF-I/Q-TEQ iteration is insignificant compared to that of the remaining RBF based iterations. Hence, we should compare the complexity of the RBF-DFE assisted scheme using seven iterations in the eight-iteration aided RBF-I/Q-TEQ-TTCM scheme shown in Figure 7, to that of the four-iteration full RBF-TEQ-TTCM scheme shown in Figure 7. Therefore, it can be shown that complexity reduction factors of $\frac{4}{7} \cdot \frac{20704}{328} \approx 36$ and $\frac{4}{7} \cdot \frac{512}{32} \approx 9$ were obtained in terms of the required number of additions/subtractions and multiplications/divisions, respectively.

Specifically, as shown in Figure 7, the 3 BPS throughput RBF-I/Q-TEQ-TTCM scheme employing eight iterations required an $E_b/N_0$ of about 14.85 dB at BER=$10^{-5}$ when communicating over dispersive two-path Rayleigh fading channels. By contrast, the identical 3 BPS throughput uncoded 8PSK AWGN benchmarker and the conventional DFE assisted uncoded 8PSK scheme communicating over the dispersive two-path Rayleigh fading channels required an $E_b/N_0$ of 12.97 dB and 31.63 dB, respectively, at a BER of $10^{-5}$. Therefore, the RBF-I/Q-TEQ-TTCM scheme employing eight iterations, required only about 14.85-12.97 = 1.88 dB higher SNR at BER=$10^{-5}$, than the identical throughput 3 BPS uncoded 8PSK AWGN benchmarker. The coding gain of the scheme is about 31.63-14.85=16.78 dB at BER=$10^{-5}$.

## 4. CONCLUSION

In conclusion, the BER performance of both the 16QAM-based RBF-TEQ-CM and RBF-I/Q-TEQ-CM schemes when communicating over wideband fading channels, was found to be only about 2 dB away from the identical-throughput uncoded 8PSK scheme communicating over AWGN channels. We found that the RBF-I/Q-TEQ scheme employing LMS-based CIR estimation exhibited only marginal performance losses compared to ideal systems employing perfect CIR estimation. This is because the effect of error propagation was reduced significantly when employing RBF-I/Q-TEQ scheme, compared to that of the complex-valued RBF-TEQ scheme.

Our simulation results show significant complexity reductions for the RBF-I/Q-TEQ-CM scheme when compared to complex-valued RBF-TEQ-CM, while achieving virtually the same performance. This was demonstrated in Figure 7.

We have also compared the performance of the RBF-TEQ-CM and RBF-I/Q-TEQ-CM schemes to that of the conventional DFE assisted CM scheme, where the coding gain of the RBF-TEQ-CM and RBF-I/Q-TEQ-CM schemes is significantly higher than that of their conventional DFE based counterpart, as we have demonstrated in Sections 2 and 3. Although the complexity of RBF-TEQ is higher than that of the conventional DFE, the RBF assisted schemes are capable of maintaining a lower complexity than that of their conventional trellis-based counterparts, when communicating over both dispersive Gaussian and Rayleigh fading channels, while maintaining a similar performance [11, 14].

## 5. ACKNOWLEDGEMENTS

The financial support of the European Union under the auspices of the SCOUT project, the EPSRC, Swindon UK is

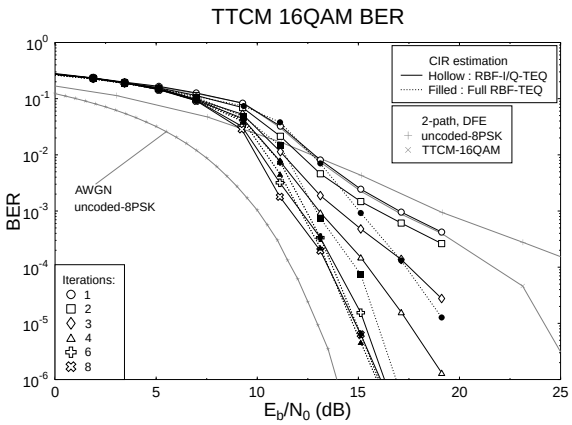


Figure 7: The BER versus $E_b/N_0$ performance of the **RBF-I/Q-TEQ-TTCM** and **RBF-TEQ-TTCM** 16QAM schemes, when communicating over the dispersive channel having an equally-weighted two-path Rayleigh fading CIR.

gratefully acknowledged.

## 6. REFERENCES


[1] G. Ungerböck, "Channel Coding with Multilevel/Phase Signals," *IEEE Transactions on Information Theory*, vol. IT-28, pp. 55–67, January 1982.

[2] C. Berrou and A. Glavieux, "Near optimum error correcting coding and decoding: Turbo codes," *IEEE Transactions on Communications*, vol. 44, pp. 1261–1271, October 1996.

[3] P. Robertson, T. Wörz, "Bandwidth-Efficient Turbo Trellis-Coded Modulation Using Punctured Component Codes," *IEEE Journal on Selected Areas in Communications*, vol. 16, pp. 206–218, February 1998.

[4] E. Zehavi, "8-PSK trellis codes for a Rayleigh fading channel," *IEEE Transactions on Communications*, vol. 40, pp. 873–883, May 1992.

[5] G. Caire and G. Taricco and E. Biglieri, "Bit-Interleaved Coded Modulation," *IEEE Transactions on Information Theory*, vol. 44, pp. 927–946, May 1998.

[6] L. Hanzo, T.H. Liew and B.L. Yeap, *Turbo Coding, Turbo Equalisation and Space Time Coding for Transmission over Wireless channels*. New York, USA: John Willy IEEE Press, 2002.

[7] S. Chen, S. McLaughlin, and B. Mulgrew, "Complex-valued radial basis function network, Part II: Application to digital communications channel equalisation," *EURASIP Signal Processing*, vol. 36, pp. 175–188, March 1994.

[8] L. Hanzo, W. Webb, and T. Keller, *Single- and Multi-carrier Quadrature Amplitude Modulation*. New York, USA: IEEE Press-John Wiley, April 2000.

[9] J. G. Proakis, "Chapter 10: Communication Through Band-Limited Channels," in *Digital Communications*, (New York), pp. 583–635, McGraw-Hill International Editions, 3rd Edition, September 1995.

[10] M. S. Yee, T. H. Liew and L. Hanzo, "Burst-by-Burst Adaptive Turbo-Coded Radial Basis Function-Assisted Decision Feedback Equalization," *IEEE Transactions on Communications*, vol. 49, pp. 1935–1945, November 2001.

[11] L. Hanzo and C. H. Wong and M. S. Yee, *Adaptive Wireless Transceivers: Turbo-Coded, Turbo-Equalized and Space-Time Coded TDMA, CDMA and OFDM Systems*. New York, USA: John Wiley, IEEE Press, 2002.

[12] M.S. Yee and L. Hanzo, "A Wideband Radial Basis Function Decision Feedback Equaliser Assisted Burst-by-burst Adaptive Modem," *IEEE Transactions on Communications*, vol. 50, pp. 693–697, May 2002.

[13] M. S. Yee, B. L. Yeap, and L. Hanzo, "Turbo equalisation of convolutional coded and concatenated space time trellis coded systems using radial basis function aided equalizers," in *Proceedings of Vehicular Technology Conference*, (Atlantic City, USA), pp. 882–886, Oct 7-11 2001.

[14] M. S. Yee and B. L. Yeap and L. Hanzo, "Radial Basis Function Assisted Turbo Equalization," *IEEE Transactions on Communications*, vol. 51, pp. 664–675, April 2003.

[15] B. L. Yeap, T. H. Liew, J. Hàmorskỳ, and L. Hanzo, "Comparative study of turbo equalisers using convolutional codes, convolutional-based turbo codes and block-based turbo codes," *IEEE Journal on Selected areas in Communications*, vol. 1, pp. 266–273, April 2002.

[16] B. L. Yeap, C. H. Wong, and L. Hanzo, "Reduced Complexity In-Phase/Quadrature-Phase M-QAM Turbo Equalization Using Iterative Channel Estimation," *IEEE Transactions on Wireless communications*, vol. 2, pp. 2–10, January 2003.

[17] C. Douillard, A. Picart, M. Jézéquel, P. Didier, C. Berrou, and A. Glavieux, "Iterative correction of intersymbol interference: Turbo-equalization," *European Transactions on Communications*, vol. 6, pp. 507–511, 1995.

[18] M. Gertsman and J. Lodge, "Symbol-by-symbol MAP demodulation of CPM and PSK signals on Rayleigh flat-fading channels," *IEEE Transactions on Communications*, vol. 45, pp. 788–799, July 1997.

[19] D. Raphaeli and Y. Zarai, "Combined turbo equalization and turbo decoding," *IEEE Communications Letters*, vol. 2, pp. 107–109, April 1998.

[20] M. Yee and L. Hanzo, "Multi-level Radial Basis Function network based equalisers for Rayleigh channel," in *Proceeding of VTC'99 (Spring)*, (Houston, TX, USA), pp. 707–711, IEEE, 16–20 May 1999.

[21] S. Chen, B. Mulgrew, and P. M. Grant, "A clustering technique for digital communications channel equalization using radial basis function networks," *IEEE Transactions on Neural Networks*, vol. 4, pp. 570–579, July 1993.

[22] S. Chen, B. Mulgrew, and S. McLaughlin, "Adaptive Bayesian equalizer with decision feedback," *IEEE Transactions on Signal Processing*, vol. 41, pp. 2918–2927, September 1993.

[23] E.-S. Chng, H. Yang, and W. Skarbek, "Reduced complexity implementation of Bayesian equaliser using local RBF network for channel equalisation problem," *Electronics Letters*, vol. 32, pp. 17–19, January 1996.

[24] S. K. Patra and B. Mulgrew, "Computational aspects of adaptive radial basis function equalizer design," in *IEEE International Symposium on Circuits and Systems, ISCAS'97*, vol. 1, pp. 521–524, IEEE, Piscataway, NJ, USA, June 1997.

[25] P. Robertson and E. Villebrun and P. Höher, "A Comparison of Optimal and Sub-Optimal MAP Decoding Algorithms Operating in the Log Domain," in *Proceedings of the International Conference on Communications*, (Seattle, United States), pp. 1009–1013, June 1995.

[26] A. Klein and R. Pirhonen and J. Skoeld and R. Suoranta, "FRAMES Multiple Access MODE 1 — Wideband TDMA with and without Spreading," in *Proceedings of the IEEE International Symposium on Personal, Indoor and Mobile Radio Communications (PIMRC)*, vol. 1, (Helsinki, Finland), pp. 37–41, 1–4 September 1997.

[27] J. G. Proakis, *Digital Communications*. Mc-Graw Hill International Editions, 3rd ed., 1995.

[28] B. L. Yeap, C. H. Wong, and L. Hanzo, "Reduced Complexity In-phase/Quadrature-phase Turbo Equalisation using Iterative Channel Estimation," *IEEE International Communications Conference 2001*, vol. 2, pp. 2–11, January 2003.

[29] A. Glavieux, C. Laot, and J. Labat, "Turbo equalization over a frequency selective channel," in *Proceedings of the International Symposium on Turbo Codes*, (Brest, France), pp. 96–102, 3-5 September 1997.